Instrument Science Report WFPC2 2009-05

# Bandwidth Stability of the WFPC2 Narrow Band and Linear Ramp Filters

P. L. Lim and J. Biretta
May 18, 2009

**ABSTRACT**

*As part of the WFPC2 close-out calibrations, we examine the stability of the bandwidths of the narrow band and linear ramp filters. We measure the FWHM of the spots produced by VISFLAT exposures using linear ramp filters crossed with narrow band filters. We do this for eight different pairings of narrow band and linear ramp filters. We then compare results from 1995 and 2008, and find negligible change in the bandpass FWHM for all eight filter pairs tested. Any change in the combined bandwidth is less than about 1% of the bandwidth. Our constraints on any changes in the narrow band filters (taken alone) are less strong, but we can rule out bandwidth changes larger than about 5% for typical narrow band filters (16% for the narrowest filter, F656N).*

## 1. Introduction

The WFPC2 narrow band (NB) and linear ramp filters (LRFs) both employed thin-film technology in their constructions. The stability of such filters is not guaranteed, and depends on the poorly known and proprietary details of the manufacturing process. A previous ISR (WFPC2 ISR 09-04; hereinafter BL09) examined the stability of their central wavelengths. Herein we use a similar approach to examine the stability of their bandwidths. The

Operated by the Association of Universities for Research in Astronomy, Inc., for the National Aeronautics and Space Administration

bandwidth is a critical parameter for the filters, because photometric calibrations of continuum sources (SYNPHOT tables, etc.) would be compromised if the filter bandpass were unstable, i.e., if the width of the bandpass changed over time. The filter widths are also critical for observations of red-shifted emission line targets or other situations where the emission line is offset from the nominal filter center.

While observations of standard stars have been made on-orbit to monitor the photometric throughput of the filters, these data alone are not sufficient to completely characterize the filters. Throughput changes could arise from both changes in the peak transmission and/or widths of the filters. Moreover, there are various scenarios in which integrated throughput might remain unchanged (i.e., standard star results unchanged) even if filter peak transmission and widths were varying. For these reasons, it is important to consider the filter bandwidth as a separate parameter whose stability is important.

We use the full width at half maximum (FWHM) of a spot produced on the detector by crossing a LRF with a NB filter to characterize the filter widths. Such study is possible with this kind of filter pairing because the central wavelength and bandpass of the LRFs are dispersed along ramp (wavelength) direction in the focal plane. By comparing the FWHM values of the same filter pair early and late in the WFPC2 mission, we are able to quantify the bandwidth stability of the crossed filters, and thus infer whether or not the filters have been stable. This method is applied to eight such pairings of LRF and NB filters.

We will discuss our data and analysis in Sections 2 and 3 respectively. Then we summarize our results in Section 4.

## 2. Observations and Data Reduction

We use the fully-reduced images from our calibration work on wavelength stability for LRFs and NB filters in BL09. The exposures are all VISFLATs from proposals 6140 and 11038, which are from epochs 13 years apart. All four chips of each exposure are mosaicked together for positional measurements. For simplicity, we only use un-rotated linear ramp filters without truncated illumination profiles in the λ-direction (analogous to X-direction in BL09). Please refer to Sections 2 and 3 in BL09 for complete details of the images.

## 3. Analysis and Discussions

We used the methods and results from Section 4.1 in BL09, particularly the collapsed 1-D spot profiles and their respective Gaussian fittings in the λ-direction. An example is shown in Figure 1: Blue dashed curve is the observed 1-D spot profile; yellow region covers the subset of the profile used for fitting; red curve is the Gaussian fit; and red vertical line marks the Gaussian centroid. The FWHM (blue arrows) is derived from the X-positions of the half-

maximum points of the Gaussian which has been fitted to the 1-D profile. The fitting region is generally confined between the half-maximum points to minimize issues at CCD and field-of-view boundaries.

**Figure 1:** Example Gaussian fitting in the λ-direction for dataset FR418N×F437N for Proposal 6140. See text in Section 3 for details.

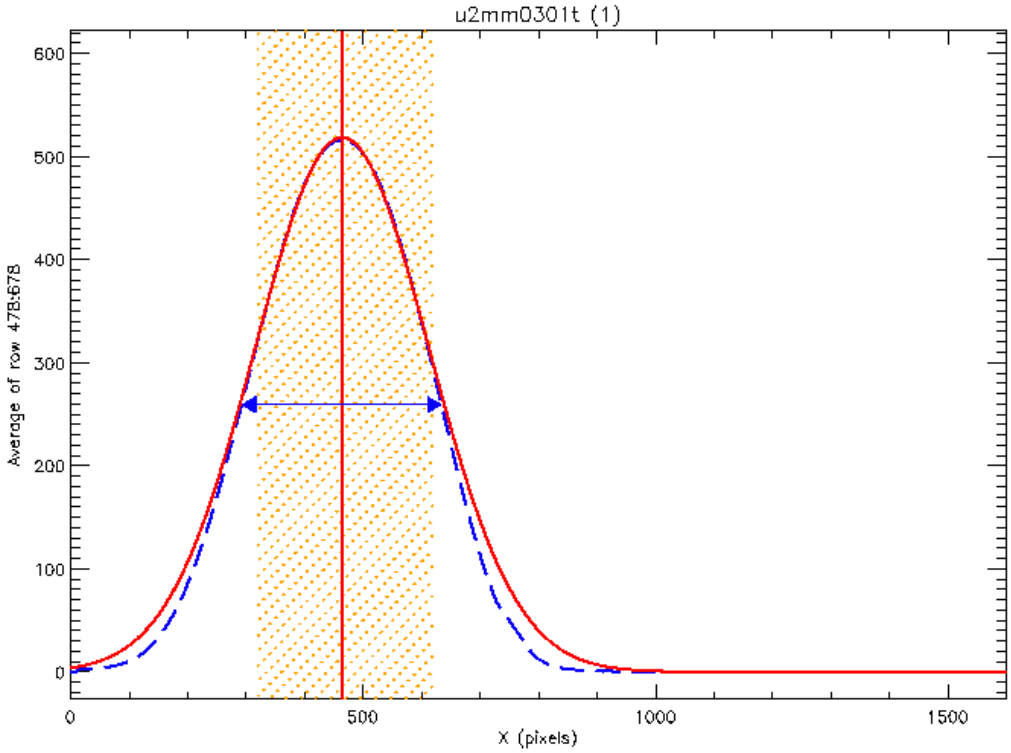


We used the LRF Calculator[1] algorithm to convert pixel locations to wavelengths, first converting mosaicked coordinates to RA & DEC with IRAF task "*xy2rd*," then to native chip coordinates with "*invmetric*." The chip coordinates were then used with the LRF Calculator algorithm to derive the wavelengths at the lower and upper half-maximum points.

For the spot centroid, which is related to the central wavelength, we used measurements from Table 3 in BL09. The Y-position of the spot (i.e., in the spatial direction) is needed for the LRF Calculator algorithm, though the value need not be very accurate; for all the calculations we assumed the same mosaicked Y-positions as the spot centroid. The X-positions of the FWHM points were derived as described above.

The mosaicked coordinates of the centroid and FWHM points are tabulated in Table 1, while their respective native chip coordinates are in Table 2. The notations "Left" or "L" and "Right" or "R" denote half-maximum points to lower and higher X, respectively.

[1] http://www.stsci.edu/hst/wfpc2/software/wfpc2_lrfcalc.html

**Table 1:** Measured centroid and FWHM positions in mosaicked coordinates.

| Image Name | Ramp Filter | NB Filter | $X_{centroid}$ (pixel) | $Y_{centroid}$ (pixel) | $X_{FWHM,L}$ (pixel) | $X_{FWHM,R}$ (pixel) |
|---|---|---|---|---|---|---|
| u2mm0101t | FR418N | F375N | 1274.5 | 1493.5 | 1088.5 | 1454.0 |
| u9w10801m | FR418N | F375N | 1287.9 | 1479.5 | 1101.0 | 1469.0 |
| u9w10802m | FR418N | F375N | 1287.1 | 1479.4 | 1101.0 | 1468.0 |
| u2mm0301t | FR418N | F437N | 465.0 | 574.8 | 293.0 | 635.0 |
| u9w10803m | FR418N | F437N | 458.5 | 574.5 | 287.0 | 629.0 |
| u2mm0401t | FR533N | F487N | 843.8 | 88.7 | 666.5 | 1024.5 |
| u9w10905m | FR533N | F487N | 847.9 | 87.5 | 669.5 | 1030.0 |
| u2mm0602t | FR680N | F631N | 1060.6 | 103.4 | 890.0 | 1232.5 |
| u9w11005m | FR680N | F631N | 1060.9 | 101.6 | 890.5 | 1233.0 |
| u2mm0603t | FR680N | F656N | 917.5 | 589.0 | 757.0 | 1087.0 |
| u9w11006m | FR680N | F656N | 921.9 | 573.5 | 760.0 | 1091.5 |
| u2mm0604t | FR680N | F658N | 830.7 | 589.0 | 670.5 | 995.5 |
| u9w11007m | FR680N | F658N | 833.7 | 571.7 | 673.5 | 999.0 |
| u2mm0605t | FR680N | F673N | 349.5 | 581.1 | 165.0 | 533.0 |
| u9w11008m | FR680N | F673N | 353.8 | 569.1 | 169.0 | 537.0 |
| u2mm0903p | FR868N | F953N | 931.9 | 126.9 | 760.0 | 1109.5 |
| u9w1100fm | FR868N | F953N | 922.6 | 125.4 | 751.0 | 1099.5 |

**Table 2:** Measured centroid and FWHM positions in native chip coordinates (pixels). The chip they belong to are also provided.

| Image Name | Ramp Filter | NB Filter | Centroid | | | FWHM (Left) | | | FWHM (Right) | | |
|---|---|---|---|---|---|---|---|---|---|---|---|
| | | | Chip | X | Y | Chip | X | Y | Chip | X | Y |
| u2mm0101t | FR418N | F375N | WF4 | 572.6 | 752.0 | WF4 | 385.6 | 754.5 | WF4 | 754.3 | 750.5 |
| u9w10801m | FR418N | F375N | WF4 | 585.8 | 737.7 | WF4 | 397.9 | 740.1 | WF4 | 769.3 | 736.1 |
| u9w10802m | FR418N | F375N | WF4 | 585.0 | 737.6 | WF4 | 397.9 | 740.0 | WF4 | 768.2 | 736.0 |
| u2mm0301t | FR418N | F437N | WF2 | 344.9 | 235.1 | WF2 | 517.1 | 235.0 | WF2 | 174.5 | 234.9 |
| u9w10803m | FR418N | F437N | WF2 | 351.4 | 235.4 | WF2 | 523.1 | 235.2 | WF2 | 180.6 | 235.2 |
| u2mm0401t | FR533N | F487N | WF3 | 730.8 | 126.4 | WF2 | 142.1 | 722.9 | WF3 | 731.1 | 308.6 |
| u9w10905m | FR533N | F487N | WF3 | 732.0 | 130.5 | WF2 | 139.1 | 724.2 | WF3 | 732.4 | 314.1 |
| u2mm0602t | FR680N | F631N | WF3 | 716.5 | 344.9 | WF3 | 716.0 | 173.3 | WF3 | 717.6 | 517.6 |
| u9w11005m | FR680N | F631N | WF3 | 718.3 | 345.2 | WF3 | 717.8 | 173.8 | WF3 | 719.5 | 518.1 |
| u2mm0603t | FR680N | F656N | WF3 | 228.5 | 204.5 | WF2 | 51.5 | 220.3 | WF3 | 229.7 | 374.4 |
| u9w11006m | FR680N | F656N | WF3 | 244.1 | 208.8 | WF2 | 48.6 | 235.8 | WF3 | 245.2 | 378.9 |
| u2mm0604t | FR680N | F658N | WF3 | 227.7 | 117.1 | WF2 | 138.8 | 220.5 | WF3 | 229.0 | 282.8 |
| u9w11007m | FR680N | F658N | WF3 | 245.1 | 120.1 | WF2 | 135.8 | 237.9 | WF3 | 246.4 | 286.2 |
| u2mm0605t | FR680N | F673N | WF2 | 460.5 | 228.7 | WF2 | 645.7 | 228.2 | WF2 | 276.8 | 228.7 |
| u9w11008m | FR680N | F673N | WF2 | 456.2 | 240.8 | WF2 | 641.7 | 240.4 | WF2 | 272.9 | 240.8 |
| u2mm0903p | FR868N | F953N | WF3 | 692.3 | 215.7 | WF2 | 47.8 | 684.8 | WF3 | 693.0 | 394.2 |
| u9w1100fm | FR868N | F953N | WF3 | 693.8 | 206.4 | WF2 | 56.9 | 686.3 | WF3 | 694.5 | 384.2 |

For the centroid and each side of FWHM, we separately converted their respective native chip coordinates to wavelengths using the LRF Calculator algorithm, which employs information from Tables 3.7 and 3.8 in WFPC2 Instrument Handbook (McMaster, Biretta, et al. 2008; hereafter IHB). The centroid produced the measured central wavelength, $\lambda_c$. Then we calculated the FWHM by subtracting the wavelengths obtained from each side of FWHM positions. Finally, we computed the percentage dimensionless width, *w*, using Equation 1 below.

$$w = 100\% \times FWHM / \lambda_c \quad (1)$$

We tabulate our results in Table 3. The measured widths, *w,* are typically in the range of 1.3-1.7%, and correspond well with the nominal widths of the LRFs (~1.3%) convolved with a somewhat narrower NB filter (0.5-1.0%). For each filter pair, the change in *w* from 1995 to 2008 is about 0.01% or less. When expressed as a fraction of the bandwidth, the change in FWHM is typically less than 1% of the bandwidth.

**Table 3:** FWHM stability check results measured from VISFLAT datasets.

| Image Name | Ramp Filter | NB Filter | Obs. Date (Y-M-D) | Prop. ID | $\lambda_c$ (Å) | FWHM (Å) | *w* (%) |
|---|---|---|---|---|---|---|---|
| u2mm0101t | FR418N | F375N | 1995-02-25 | 6140 | 3737.133 | 56.393 | 1.509 |
| u9w10801m | FR418N | F375N | 2008-01-24 | 11038 | 3735.107 | 56.789 | 1.520 |
| u9w10802m | FR418N | F375N | 2008-01-24 | 11038 | 3735.235 | 56.631 | 1.516 |
| u2mm0301t | FR418N | F437N | 1995-02-25 | 6140 | 4376.547 | 62.488 | 1.428 |
| u9w10803m | FR418N | F437N | 2008-01-24 | 11038 | 4377.736 | 62.486 | 1.427 |
| u2mm0401t | FR533N | F487N | 1995-02-22 | 6140 | 4864.793 | 67.844 | 1.395 |
| u9w10905m | FR533N | F487N | 2008-01-23 | 11038 | 4864.013 | 68.320 | 1.405 |
| u2mm0602t | FR680N | F631N | 1995-03-01 | 6140 | 6301.887 | 101.495 | 1.611 |
| u9w11005m | FR680N | F631N | 2008-01-25 | 11038 | 6301.959 | 101.495 | 1.611 |
| u2mm0603t | FR680N | F656N | 1995-03-01 | 6140 | 6560.514 | 99.303 | 1.514 |
| u9w11006m | FR680N | F656N | 2008-01-25 | 11038 | 6559.253 | 99.766 | 1.521 |
| u2mm0604t | FR680N | F658N | 1995-03-01 | 6140 | 6586.954 | 97.976 | 1.487 |
| u9w11007m | FR680N | F658N | 2008-01-25 | 11038 | 6586.102 | 98.146 | 1.490 |
| u2mm0605t | FR680N | F673N | 1995-03-01 | 6140 | 6732.173 | 111.585 | 1.657 |
| u9w11008m | FR680N | F673N | 2008-01-25 | 11038 | 6730.919 | 111.564 | 1.657 |
| u2mm0903p | FR868N | F953N | 1995-03-07 | 6140 | 9535.076 | 147.262 | 1.544 |
| u9w1100fm | FR868N | F953N | 2008-01-25 | 11038 | 9531.115 | 146.877 | 1.541 |

Assuming negligible error in coordinate conversion and LRF Calculator, we took 1- and 2-pixel uncertainties in mosaicked X and Y positions, respectively, from Section 4.3 in BL09. Then we added these errors to our mosaicked coordinates in Table 1 and calculated the deviations in resultant *w* values compared to Table 3. From this exercise, we estimated the uncertainties in the widths to be ~0.01%. Hence the changes in width between the different epochs are within measurement uncertainties, and there appear to be no significant change in FHWM for these eight filter pairs.

In general, the NB filters are narrower than the LRF filters, so that our measurements of the convolved bandpasses are more sensitive to changes in the LRF FWHM than those of the NB filters. For the narrowest of the NB filters tested, F656N, the NB filter FWHM is about one-fourth that of the LRF filter. If we assume Gaussian profiles for both filters, our measurement uncertainty implies that we could detect only changes larger than about 16% in the FWHM of F656N. For wider and more typical NB filter widths, such as F487N, we are sensitive to changes larger than about 5% of the FWHM. The sensitivity to the NB filter width depends on the detailed shape of the bandpasses. The Gaussian profile assumed here gives the least

sensitivity to changes in the NB filter, while some other shape (e.g., a box-car) would give higher sensitivity to any changes in the NB filter.

It is also interesting to compare the filter widths measured here with those published in the IHB. Before making this comparison, we must first convolve the IHB bandwidths for the LRF and NB filters that were used when taking the VISFLATs. We calculated the LRF widths from the IHB, $w_{LRF}$, using coefficients from Tables 3.2 to 3.6 and the equations in Section 3.3.1. These values are from ramp filters measured in a laboratory circa 1992 (also see Figure 3.4 in IHB). We obtained widths for NB filters, $w_{NB}$, from Table 3.1 in the IHB using their $\overline{\lambda}$ and $\Delta\overline{\lambda}$ values. Then we calculated convolved widths assuming Gaussian and box-car bandpass profiles, as shown in Equations 2 and 3 below, respectively.

$$w_G = \sqrt{{w_{LRF}}^2 + {w_{NB}}^2} \tag{2}$$

$$w_{BC} = w_{LRF} + w_{NB} \tag{3}$$

These values are tabulated in Table 4. As the actual bandpass shapes lie somewhere between Gaussian and box-car (see Appendix A in the IHB), we expect the observed widths to have values between $w_G$ and $w_{BC}$. This is indeed the case for the $w$ values in Table 3 (restated as $w_{1995}$ and $w_{2008}$ in Table 4 for clarity). This gives us some confidence that our results are reasonable and some confirmation of the filter properties listed in the IHB.

**Table 4:** Percentage dimensionless widths for comparison. The $w_{1995}$ and $w_{2008}$ values are taken from the corresponding $w$ in Table 3. See text for details.

| Ramp Filter | NB Filter | $w_{LRF}$ (%) | $w_{NB}$ (%) | $w_G$ (%) | $w_{BC}$ (%) | $w_{1995}$ (%) | $w_{2008}$ (%) |
|---|---|---|---|---|---|---|---|
| FR418N | F375N | 1.186 | 0.654 | 1.354 | 1.840 | 1.509 | 1.518[a] |
| FR418N | F437N | 1.085 | 0.577 | 1.229 | 1.662 | 1.428 | 1.427 |
| FR533N | F487N | 1.110 | 0.532 | 1.231 | 1.642 | 1.395 | 1.405 |
| FR680N | F631N | 1.313 | 0.490 | 1.401 | 1.803 | 1.611 | 1.611 |
| FR680N | F656N | 1.277 | 0.328 | 1.318 | 1.605 | 1.514 | 1.521 |
| FR680N | F658N | 1.280 | 0.432 | 1.351 | 1.712 | 1.487 | 1.490 |
| FR680N | F673N | 1.301 | 0.701 | 1.478 | 2.002 | 1.657 | 1.657 |
| FR868N | F953N | 1.304 | 0.550 | 1.415 | 1.854 | 1.544 | 1.541 |

[a] Average of FR418N×F375N $w$ values for 2008.

## 4. Summary

We used VISFLAT data from Biretta & Lim 2009, observed in 1995 and 2008, in which LRFs were crossed with NB filters, to assess the stability of the filter bandwidths. From Gaussian fitting to the spot profiles, we obtained central wavelengths and FWHM values, which we used to measure changes in the combined filter widths over the 13 years.

The dimensionless filter widths, *w*, from different epochs for the same filter combination changed by 0.01% or less for the eight filter pairings studied. Expressed as a fraction of the bandwidth, the changes are less than ~1% of the combined bandwidth and are consistent with the uncertainty from the fitting procedure.

Since the NB filters are generally narrower than the LRFs, our method is less sensitive to changes in the NB filters, but we can still state that any changes in the NB filter bandwidths are typically less than 5% of the bandwidth (or less than 16% for the narrowest of the NB filters, F656N).

As a consistency check, we compared our FWHM values with those expected for simple transmission profile convolutions (Gaussian and box-car) of the published LRF and NB filter widths and find good agreement. This gives some confirmation of our measurement methods and the published values.

In conclusion, the bandwidths for all eight filter pairings studied in this report appear stable over the span of 13 years. Any changes in either the LRFs or the NB filters are typically small and would have minimal effect on science observations.

## Acknowledgements

We thank Dr. Van Dixon, who reviewed this report and provided insightful feedback.

## References

Biretta, J., & Lim, P. L. 2009, "Wavelength Stability of the WFPC2 Narrow Band and Linear Ramp Filters," WFPC2 Instrument Science Report 09-04.

McMaster, M., Biretta, J., et al. 2008, WFPC2 Instrument Handbook, Version 10.0 (Baltimore: STScI)